

Optical IFU Observations of GOALS Sample with KOOLS-IFU on Seimei Telescope: Initial results of 9 U/LIRGs at $z < 0.04$

Yoshiki TOBA^{1,2,3,4,5,*†}, Satoshi YAMADA^{6,2}, Kazuya MATSUBAYASHI^{7,8}, Koki TERAO^{9,10}, Aoi MORIYA³, Yoshihiro UEDA², Kouji OHTA², Aoi HASHIGUCHI³, Kazuharu G. HIMOTO¹¹, Hideyuki IZUMIURA¹², Kazuma JOH¹¹, Nanako KATO¹¹, Shuhei KOYAMA^{7,5}, Hiroyuki MAEHARA¹², Rana MISATO³, Akatoki NOBORIGUCHI^{13,10,11}, Shoji OGAWA², Naomi OTA³, Mio SHIBATA³, Nozomu TAMADA¹¹, Anri YANAGAWA³, Naoki YONEKURA¹¹, Tohru NAGAO⁵, Masayuki AKIYAMA¹⁰, Masaru KAJISAWA^{5,11}, Yoshiki MATSUOKA⁵

¹National Astronomical Observatory of Japan, 2-21-1 Osawa, Mitaka, Tokyo 181-8588, Japan

²Department of Astronomy, Kyoto University, Kitashirakawa-Oiwake-cho, Sakyo-ku, Kyoto 606-8502, Japan

³Department of Physics, Nara Women's University, Kitauoyanishi-machi, Nara, Nara 630-8506, Japan

⁴Academia Sinica Institute of Astronomy and Astrophysics, 11F of Astronomy-Mathematics Building, AS/NTU, No.1, Section 4, Roosevelt Road, Taipei 10617, Taiwan

⁵Research Center for Space and Cosmic Evolution, Ehime University, 2-5 Bunkyo-cho, Matsuyama, Ehime 790-8577, Japan

⁶RIKEN Cluster for Pioneering Research, 2-1 Hirose, Wako, Saitama 351-0198, Japan

⁷Institute of Astronomy, Graduate School of Science, The University of Tokyo, 2-21-1 Osawa, Mitaka, Tokyo 181-0015, Japan

⁸Okayama Observatory, Kyoto University, Honjo 3037-5, Kamogata-cho, Asakuchi, Okayama 719-0232, Japan

⁹Subaru Telescope, National Astronomical Observatory of Japan, 650 North A'ohoku Place, Hilo, HI 96720, USA

¹⁰Astronomical Institute, Tohoku University, Aramaki, Aoba-ku, Sendai, 980-8578, Japan

¹¹Graduate School of Science and Engineering, Ehime University, Bunkyo-cho, Matsuyama 790-8577, Japan

¹²Okayama Branch Office, Subaru Telescope, National Astronomical Observatory of Japan, NINS, Kamogata, Asakuchi, Okayama 719-0232, Japan

¹³School of General Education, Shinshu University, 3-1-1 Asahi, Matsumoto, Nagano 390-8621, Japan

*E-mail: yoshiki.toba@nao.ac.jp

Received (2022 April 20); Accepted (2022 August 22)

Abstract

We present ionized gas properties of 9 local ultra/luminous infrared galaxies (U/LIRGs) at $z < 0.04$ through IFU observations with KOOLS-IFU on Seimei Telescope. The observed targets are drawn from the Great Observatories All-sky LIRG Survey (GOALS), covering a wide range of merger stages. We successfully detect emission lines such as $H\beta$, $[\text{O III}]\lambda 5007$, $H\alpha$,

[N II] $\lambda\lambda$ 6549,6583, and [S II] $\lambda\lambda$ 6717,6731 with a spectral resolution of $R = 1500\text{--}2000$, which provides (i) spatially-resolved ($\sim 200\text{--}700$ pc) moment map of ionized gas and (ii) diagnostics for active galactic nucleus (AGN) within the central $\sim 3\text{--}11$ kpc in diameter for our sample. We find that [O III] outflow that is expected to be driven by AGN tends to be stronger (i) towards the galactic center and (ii) as a sequence of merger stage. In particular, the outflow strength in the late-stage (stage D) mergers is about 1.5 times stronger than that in the early-stage (stage B) mergers, which indicates that galaxy mergers could induce AGN-driven outflow and play an important role in the co-evolution of galaxies and supermassive black holes.

Key words: galaxies: active — infrared: galaxies — methods: observational

1 Introduction

In the last two decades, galaxy mergers have been recognized as a key phenomenon for understanding galaxy evolution (e.g., Conselice 2014 and reference therein). Star formation (SF) and/or active galactic nucleus (AGN) activity in galaxies are often triggered by galaxy mergers¹, which enhances the inflow of material from galactic scales into the close environments of the nuclear region. The galaxy merger also enhances infrared (IR) luminosity (L_{IR}^2) (e.g., Sanders et al. 1988; Veilleux et al. 2002; Imanishi et al. 2007; Imanishi 2009; Toba et al. 2015; Toba & Nagao 2016; Toba et al. 2017a). These are observed as luminous IR galaxies (LIRGs) and ultraluminous IR galaxies (ULIRGs) with L_{IR} greater than 10^{11} and $10^{12} L_{\odot}$, respectively (Sanders & Mirabel 1996). Recent works also suggested that the relative strength of SF and AGN activity in U/LIRGs may be varied in the course of galaxy mergers (e.g., Narayanan et al. 2010; Ricci et al. 2017; Blecha et al. 2018; Yamada et al. 2019; Yamada et al. 2021). In particular, radiation from an AGN is expected to interact with the interstellar medium (ISM) and lead to the ejection or heating of the gas, which could be tightly associated with the growth of the galaxy and its supermassive black hole (SMBH) (e.g., Cazzoli et al. 2016; Toba et al. 2017b; Harrison et al. 2018; Chen et al. 2019; Finnerty et al. 2020; Jun et al. 2020; Fluetsch et al. 2021). That AGN-driven outflow is often observed in U/LIRGs: recent observations reported that dusty IR luminous AGN often shows a strong ionized gas outflow, and its strength seems to be correlated with L_{IR} (Bischetti et al. 2017; Toba et al. 2017c; Chen et al. 2019; Jun et al. 2020). Therefore, U/LIRGs are a good laboratory to

examine how AGN-driven outflow could influence the host galaxy and its SMBH. However, those works are often limited to handling a whole galaxy as a system. To address, from a spatially-resolved point of view, how the SF and AGN activity could be enhanced/quenched as a function of merger sequence, Integral Field Unit (IFU) observation is a quite powerful tool that may trace the gas kinematics and energetics (e.g., Bae et al. 2017; Shin et al. 2019; Pan et al. 2019).

In this work, we focus on the Great Observatories All-sky LIRG Survey (GOALS; Armus et al. 2009) that provides a complete, flux-limited (i.e., flux density at $60 \mu\text{m} > 5.24$ Jy) U/LIRG sample in the local universe. In addition to their multi-wavelength follow-up observations, Stierwalt et al. (2013) divided the GOALS U/LIRGs into subsamples regarding the merger stage, based on a visual inspection of the IRAC/Spitzer $3.6 \mu\text{m}$ images and/or higher resolution images taken by e.g., Hubble Space Telescope (see also Haan et al. 2011). Therefore, the GOALS sample is an ideal laboratory to investigate the role of galaxy mergers in the co-evolution of galaxies and SMBHs.

In this paper, we present the initial results of our follow-up campaign of GOALS sample with an optical IFU, the Kyoto Okayama Optical Low-dispersion Spectrograph with optical-fiber IFU (KOOLS-IFU; Yoshida 2005; Matsubayashi et al. 2019) on the Okayama 3.8 m, Seimei Telescope (Kurita et al. 2020). The structure of this paper is as follows. Section 2 describes the sample selection, observations, and data reduction of observed targets. In Section 3, we present the results of our optical IFU observations and discuss the dependence of ionized gas outflow on distance from the galaxy center and merger stage. We summarize the results of this work in Section 4. Throughout this paper, the adopted cosmology is a flat universe with $H_0 = 70 \text{ km s}^{-1} \text{ Mpc}^{-1}$, $\Omega_{\text{M}} = 0.28$, and $\Omega_{\Lambda} = 0.72$, which are the same as those adopted in a series of GOALS papers that are relevant to this work (e.g., Armus et al. 2009; Rich et al. 2015).

[†] NAOJ Fellow

¹ We note that major mergers are not the only triggering mechanism of SF/AGN activity. Non-merger processes such as secular mechanisms may also trigger SF/AGN activity (see e.g., Schawinski et al. 2011; Draper & Ballantyne 2012; Sharma et al. 2021, and references therein) (see also Section 3.4).

² L_{IR} is empirically defined as the luminosity integrated over a wavelength range of $8\text{--}1000 \mu\text{m}$ (e.g., Sanders & Mirabel 1996; Chary & Elbaz 2001).

2 Data and analysis

2.1 Target selection

The observed targets were drawn from the GOALS sample, which is itself a subset of the IRAS Revised Bright Galaxy Sample (Sanders et al. 2003), providing a 60 μm flux-limited sample of U/LIRGs at $z < 0.088$. The GOALS sample has been extensively examined by multi-wavelength observations from X-ray (e.g., Iwasawa et al. 2011; Ricci et al. 2017; Torres-Albà et al. 2018; Yamada et al. 2020; Ricci et al. 2021; Yamada et al. 2021), ultraviolet (UV) (e.g., Howell et al. 2010; Petty et al. 2014), optical-NIR (e.g., Haan et al. 2011; Kim et al. 2013; Linden et al. 2017; Jin et al. 2019; Larson et al. 2020), mid-IR (MIR)–far-IR (FIR) (e.g., Inami et al. 2013; Stierwalt et al. 2013; Stierwalt et al. 2014; Chu et al. 2017; Díaz-Santos et al. 2017; Inami et al. 2018; Yamada et al. 2019; Armus et al. 2020) to radio (e.g., Privon et al. 2015; Barcos-Muñoz et al. 2017; Yamashita et al. 2017; Herrero-Illana et al. 2019; Linden et al. 2019; Condon et al. 2021) (see also Casey 2012; U et al. 2012 for SED analysis). We employed the merger classifications provided by Stierwalt et al. (2013), which have five categories from **N** (no signs of merger activity or massive neighbors), to stage **A** (galaxy pairs prior to a first encounter), **B** (post-first encounter with galaxy disks that are still symmetric and intact but with signs of tidal tails), **C** (showing amorphous disks, tidal tails, and other signs of merger activity), and **D** (two nuclei in a common envelope), as a sequence of merger stage (see Section 2.5 in Stierwalt et al. 2013 for more detail) (see also e.g., Figure 1 in Ricci et al. 2017 for an example image of each merger stage).

We selected 9 objects as the target by taking into account the magnitude in optical bands ($r\text{-mag} < 16.0$), merger stage, previous IFU observations, and visibility from the Seimei telescope. The basic information of observed targets is summarized in Table 1. Figure 1 shows distributions of redshift, IR luminosity, and merger stage of our sample. We also present those distributions for all the GOALS sample (Armus et al. 2009) and sub-sample reported in Rich et al. (2015), who performed the IFU observations of 27 southern U/LIRGs from the GOALS sample with the Wide Field Spectrograph (WiFeS) installed on a 2.3 m telescope that capability is similar to KOOLS-IFU. We confirm from Figure 1 that our sample is widely distributed in terms of IR luminosity and merger stage while that is biased toward low- z ($z < 0.04$). Figure 2 shows i -band images of our sample taken by Pan-STARRS³ (Chambers et al. 2016).

³<https://ps1images.stsci.edu/cgi-bin/ps1cutouts>

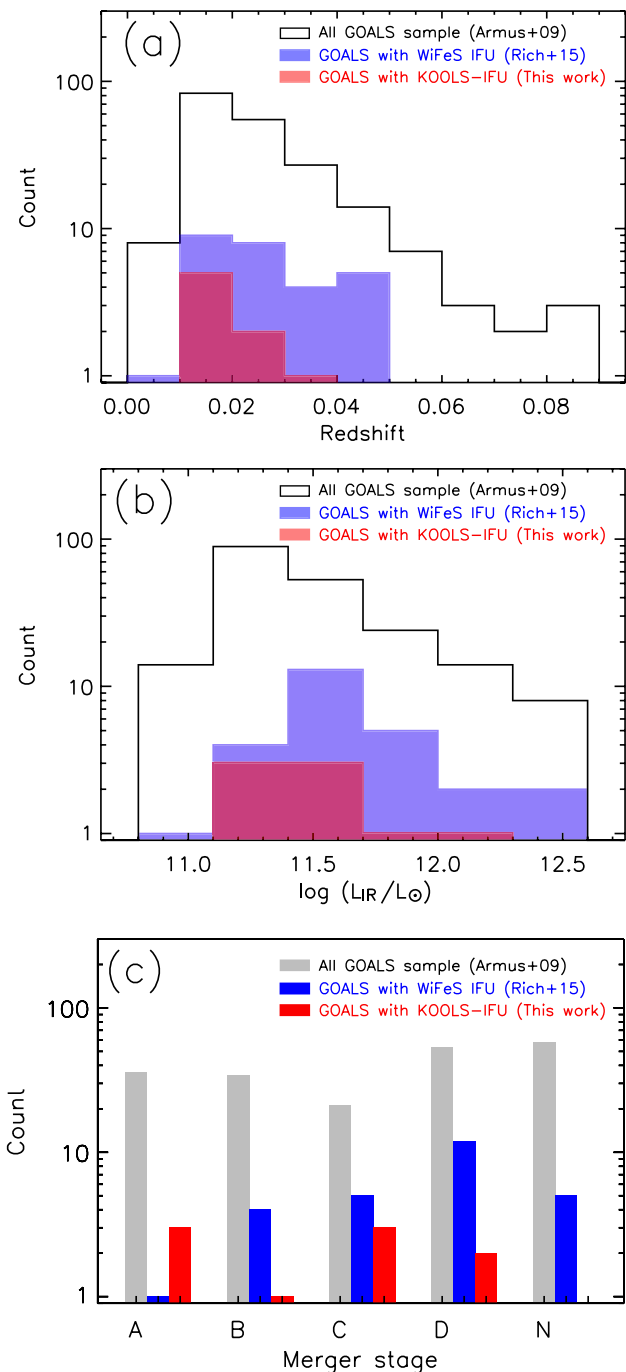


Fig. 1. Histograms of (a) redshift, (b) IR luminosity, and (c) merger stage of the GOALS sample (black/gray), GOALS sample with WiFeS provided in (Rich et al. 2015) (blue), and GOALS sample with KOOLS-IFU, i.e., our sample (red).

We note that the WiFeS-GOALS IFU survey (Rich et al. 2011; Rich et al. 2012; Rich et al. 2015), the VLT-VIMOS IFU survey (Arribas et al. 2008), the PMAS IFU survey (Alonso-Herrero et al. 2009), the INTEGRAL IFU survey (García-Marín et al. 2009), VLT-SINFONI IFU survey (Piqueras López, et al. 2012), Physics of ULIRGs

Table 1. Basic properties of observed targets in GOALS sample.

Object Name	IRAS Name	R.A. (J2000.0)	Decl. (J2000.0)	redshift	D_L (Mpc)	physical scale (kpc/arcsec)	B -mag	$\log(L_{\text{IR}}/L_{\odot})$	Merger Stage
(1)	(2)	(3)	(4)	(5)	(6)	(7)	(8)	(9)	(10)
NGC 1614	F04315-0840	04:34:00.03	-08:34:44.57	0.01594	69.12	0.32	14.7	11.65	D
CGCG 468-002W	F05054+1718_W	05:08:19.71	+17:21:48.09	0.01748	75.89	0.36	15.4	(11.22)	B
NGC 3690 West	F11257+5850_W	11:28:30.78	+58:33:42.90	0.01017	43.90	0.21	11.8	(11.93)	C
NGC 3690 East	F11257+5850_E	11:28:33.39	+58:33:46.40	0.01036	44.74	0.21	11.8	(11.93)	C
Mrk 273	F13428+5608	13:44:42.07	+55:53:13.17	0.03734	164.61	0.74	15.7	12.21	D
NGC 6786	F19120+7320_W	19:10:53.75	+73:24:36.60	0.02524	110.27	0.51	13.7	(11.49)	C
NGC 6921	20264+2533_W	20:28:28.84	+25:43:24.19	0.01447	62.67	0.30	14.4	(11.11)	A
NGC 7674	F23254+0830	23:27:56.70	+08:46:44.24	0.02903	127.17	0.58	13.9	11.56	A
NGC 7679	23262+0314_W	23:28:46.67	+03:30:40.99	0.01715	74.45	0.35	13.2	11.11	A

Columns: (1) object name from SIMBAD Astronomical Database or NASA/IPAC Extragalactic Database (NED). (2) IRAS name. (3–4) right ascension (R.A.) and declination (Decl.) (J2000.0). (5) spectroscopic redshift in NED. (6–7) luminosity distance and physical size in 1 arcsec in the assumed cosmology. (8) B -band magnitude from SIMBAD or NED. (9) IR luminosity from Armus et al. (2009), where values in brackets denote the total IR luminosity for a system. (10) merger stage from Stierwalt et al. (2013).

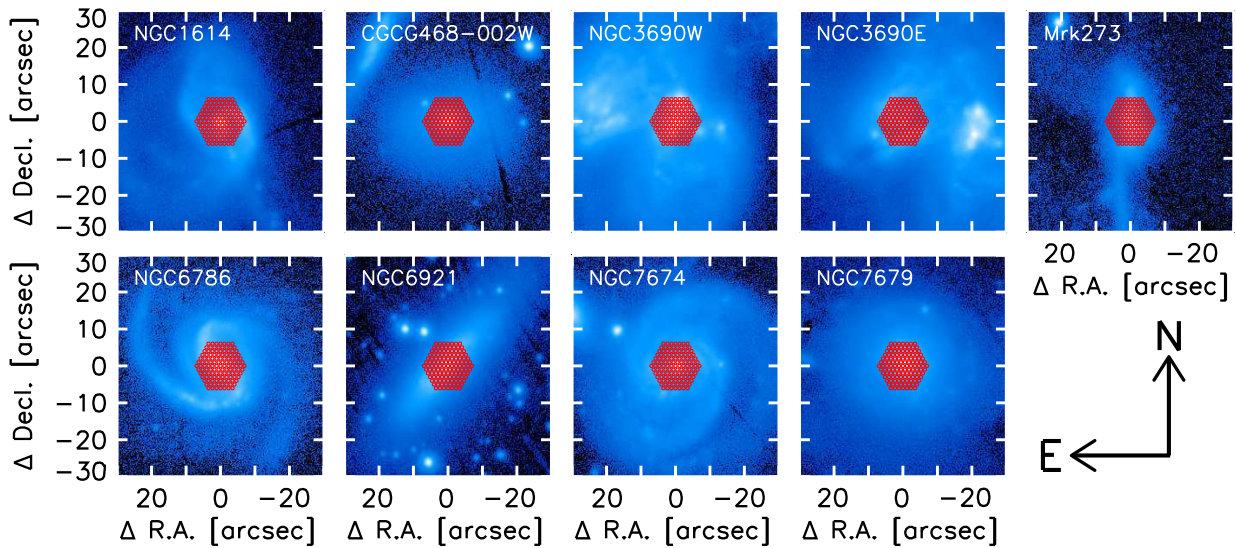


Fig. 2. The i -band postage stamps ($60'' \times 60''$) of our sample taken by Pan-STARRS. The footprint of the KOOLS-IFU with 127 fibers is overlaid as red circles. R.A. and decl. are relative coordinates with respect to those in Table 1 in which $(\Delta\text{R.A.}, \Delta\text{Decl.}) = (0, 0)$ also corresponds to the center of the field of view for KOOLS-IFU (i.e., fiber ID = 37, see Figure 3). North is up and east is left in all images.

with MUSE and ALMA (PUMA; Perna et al. 2021), and the Keck OSIRIS AO LIRG Analysis (KOALA; U et al. 2019) observed (a part of) GOALS sample (see also García-Marín et al. 2006; Rodríguez-Zaurín et al. 2011; Bellocchi et al. 2013; Arribas et al. 2014; Kakkad et al. 2022; Perna et al. 2022). In particular, the WiFeS-GOALS IFU survey provides specially-resolved maps for emission-line ratios based on various emission lines, such as $H\beta$, $[\text{O III}]\lambda 5007$, $H\alpha$, $[\text{N II}]\lambda\lambda 6549, 6583$, and $[\text{S II}]\lambda\lambda 6716, 6731$ that are also targeted lines in this work (see Section 3.2). The sample in this survey is observable from the southern hemisphere, and thus our sample (that is observable from the northern hemisphere) is complementary to those reported in Rich et al. (2015). For the remaining projects, those basically focused on one emission line (e.g., $H\alpha$) and spatially-resolved emission-line ratios

were not well investigated⁴.

2.2 Observations and data reduction

The targets were observed with the KOOLS-IFU on the Seimei Telescope in the 2019B, 2020A, and 2020B semesters (PI: Y.Toba with proposal IDs = 19B-N-CN01, 19B-K-0001, 20A-N-CN01, and 20B-K-0004). The Seimei is a new 3.8-meter diameter optical-IR alt-azimuth mount telescope located at Okayama Observatory, Kyoto

⁴ We also confirmed that our targets have not yet been cataloged in the Calar Alto Legacy Integral Field Area Survey (CALIFA; Sánchez et al. 2012) Data Release (DR) 3 (Sánchez et al. 2016), the Sydney-AAO Multi-object Integral-field spectrograph (SAMi) galaxy survey (Bryant et al. 2015) DR3 (Croom et al. 2021), and the Sloan Digital Sky Survey (SDSS; York et al. 2000) Mapping Nearby Galaxies at Apache Point Observatory survey (MaNGA; Bundy et al. 2015) DR17 (Abdurro'uf et al. 2022).

Table 2. Observation log in 2019B, 2020A, and 2020B semester.

Name	IRAS Name	Observing date	Exposure time (minutes)		Standard star
			VPH 495	VPH 683	
CGCG 468-002W	F05054+1718_W	Oct. 8, 2019	40	40	EGGR247 (=G191-B2B)
NGC 1614	F04315-0840	Oct. 9, 27, 2019	50	50	HR9087, HD74280 (=HR3454)
NGC 7679	23262+0314_W	Oct. 25, 2019	30	30	HR7596
NGC 3690 West	F11257+5850_W	Apr. 20,21, 2020	40	40	HR5501, EGGR98 (=HZ43)
NGC 3690 East	F11257+5850_E	Apr. 22,23, 2020	36	38	EGGR98 (=HZ43)
Mrk 273	F13428+5608	Apr. 23, 2020	36	36	HR5501
NGC 6786	F19120+7320_W	Aug. 16, 2020	40	40	HR7596
NGC 7674	F23254+0830	Aug 16-18, 2020	40	40	HR7596
NGC 6921	20264+2533_W	Aug. 17, 18, 2020	80	80	HD15318 (=HR718)

**Fig. 3.** The schematic view of KOOLS-IFU with fiber ID.

University, Okayama prefecture in Japan, where the typical seeing on this site is $1.2''$ – $1.4''$. The science operation was started in 2019. The KOOLS-IFU consists of 127 fibers with a total field of view (FoV) of $\sim 15''$ in diameter⁵. Each fiber is assigned a unique fiber ID as shown in Figure 3. The spatial sampling is $\sim 1.2''$ per fiber, and the 10σ limiting magnitude is 17–18 AB mag given 10 minutes of exposure. We used the VPH 495 and VPH 683⁶ grisms among four grisms equipped with the KOOLS-IFU. The wavelength coverage and the spectral resolution ($R = \lambda/\Delta\lambda$) of VPH 495 and VPH 683 are 4300–5900 Å and $R \sim 1500$ and 5800–8000 Å and $R \sim 2000$, respectively⁷. The observational log is summarized in Table 2.

The data reduction was executed with a dedicated software⁸ in which the Image Reduction and Analysis Facility (IRAF: Tody 1986; Tody 1993) tasks are utilized through the Python package (PyRAF: Science Software Branch at

STScI 2012). In particular, the IRAF `imred.hydra` package (Barden et al. 1994; Barden & Armandroff 1995) was mainly used for spectrum extraction, flat fielding, and wavelength calibration in a standard manner. Following Matsubayashi et al. (2019), spectrum extraction was done by measuring the center position of a spectrum at each pixel based on dome flat frames in which we summed the counts within ± 2.5 pixels of the center position. The wavelength was calibrated with arc (Hg and Ne) lamp frames. The flux calibration was carried out by using an observed spectrum of a standard star (see Table 2). Since we utilized all fibers of KOOLS-IFU for targets, we took sky frames separately for sky subtractions.

2.3 Spectral fitting

In order to measure the properties of emission lines such as line flux and line width for our GOALS sample, we conducted a spectral fitting to the reduced spectra by using the Quasar Spectral Fitting package (QSFIT v1.3.0⁹; Calderone et al. 2017). Following Toba et al. (2021a), we fit KOOLS-IFU spectra with the following five components; (i) AGN continuum with a single power law, (ii) Balmer continuum modeled by Grandi (1982) and Dietrich et al. (2002), (iii) host galaxy component taken from an empirical SED template in which a Spiral galaxy template¹⁰ (Polletta et al. 2007) is employed, (iv) iron blended emission lines with UV-optical templates (Vestergaard & Wilkes 2001; Véron-Cetty et al. 2004), and (v) emission lines with Gaussian components. QSFIT allows us to fit all the components simultaneously based on a Levenberg-Marquardt least-squares minimization algorithm with MPFIT (Markwardt 2009) procedure.

Since QSFIT is optimized to optical spectra taken by the SDSS (e.g., Calderone et al. 2017; Toba et al. 2021a; Toba et al. 2021b), we modified the code for general-purpose, which allows us to do the spectral fitting to KOOLS-IFU

⁵ This configuration is valid until September 2020.

⁶ We did not use an order-sorting filter O56 that is adopted for blocking the light with $\lambda < 5600$ Å.

⁷ <http://www.o.kwasan.kyoto-u.ac.jp/inst/p-kools/performance/>

⁸ <http://www.o.kwasan.kyoto-u.ac.jp/inst/p-kools/>

⁹ <https://qsfit.inaf.it>

¹⁰ We note that choice of the galaxy templates does not significantly affect the result of the fitting and our conclusion.

data. We fit the Balmer lines with narrow and broad components in which the FWHM of narrow and broad components is constrained in the range of 100–1000 km s⁻¹ and 900–15,000 km s⁻¹, respectively, to allow a good decomposition of the line profile, in the same manner as Toba et al. (2021a). Galactic extinction is corrected according to Schlafly & Finkbeiner (2011). Since one of the purposes of this work is to measure the kinematics of an ionized gas outflow, we also account for a blue-wing component of [O III]λλ4959,5007 lines. Following Calderone et al. (2017), the FWHM of the broad blue-wing component is constrained to be larger than the narrow component in the range of 100–1000 km s⁻¹ while the broad component is allowed to be blue-shifted up to 2000 km s⁻¹. The velocity offsets of [O III]λ4959 and [O III]λ5007 are tied¹¹. The measurement errors are estimated from the Monte Carlo resampling method in which we adopted the 1σ dispersion of each value by measuring them 100 times for spectra while randomly adding the noise in the same manner as in Toba et al. (2017b) (see Appendix B in Calderone et al. 2017 for a full explanation of this procedure).

3 Results and discussion

3.1 Result of the spectral fitting

Figure 4 shows examples of the optical spectral fitting with QSFit. We confirm that about 72% of the fibers are successfully fitted, of which ~90% have reduced $\chi^2 < 1.2$. This indicates that the spectra of our sample taken by KOOLS-IFU are well fitted by QSFit. The failure of the fitting is mainly due to the low SN of spectra.

3.2 Line luminosity maps and line ratio diagnostics

Figure 5 shows maps for line luminosity in units of erg s⁻¹. Luminosity is the sum of the broad and narrow emission line components as long as a broad component is detected. Otherwise, a narrow component of the emission line is used for estimating the line luminosity. Since each spectrum in fiber is fitted 100 times via the Monte Carlo realization (see Section 2.3), their weighted mean is used. Line luminosity is successfully estimated for over 95% of fibers for most objects. We note that we did not correct for internal dust extinction because it is quite hard to estimate the amount of attenuation through the Balmer decrement in all fibers due to poor SN of Hα and/or Hβ line in some fibers (see Figure 5). But this does not affect estimating the outflow

¹¹This tying could fail when the SN of the emission line is low (see e.g., the middle panels of Figure 4). In this work, we employed the velocity offset of [O III]λ5007 as long as it was reasonably measured without any warning, even if the velocity offset of [O III]λ4959 might not be securely estimated.

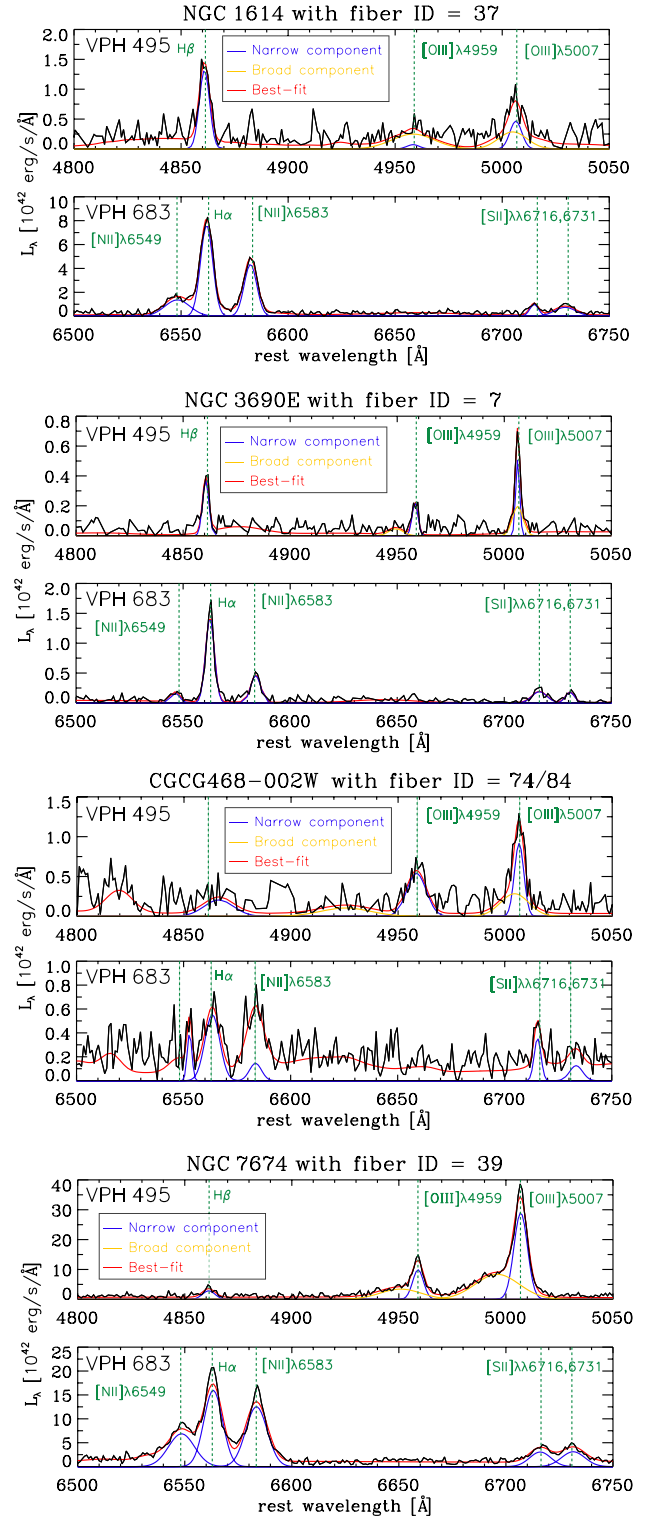


Fig. 4. Examples of spectral fitting for our objects in fiber with VPH 495 (top) and VPH 683 (bottom). The black lines are observed data. The blue and yellow curves show the narrow and broad components of emission lines, respectively. The best-fit spectrum is shown with red lines. The vertical green dashed lines correspond to the rest-frame wavelengths for Hβ, [O III]λλ4959,5007, [N II]λλ6549,6583, Hα, and [S II]λλ6716,6731 lines.

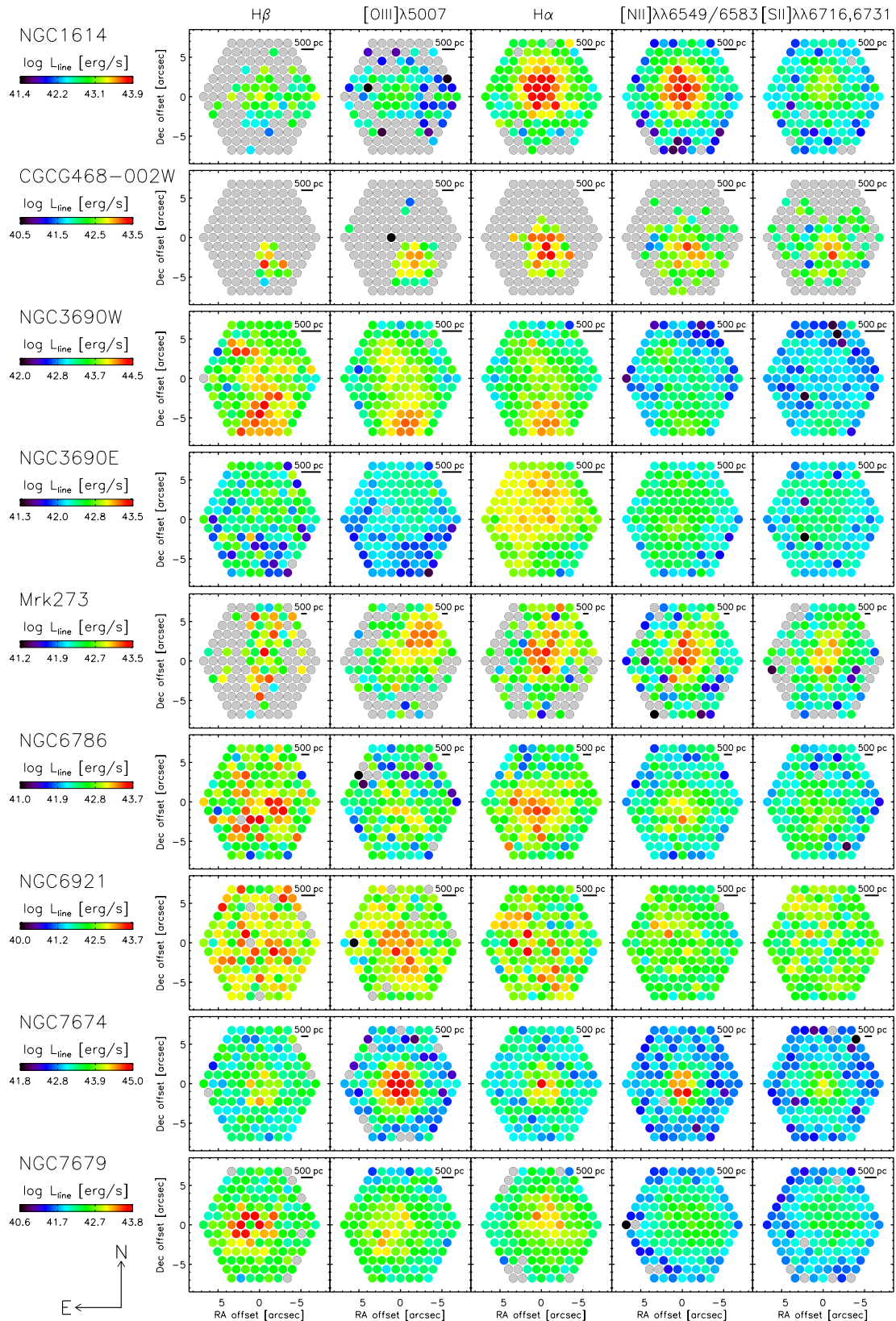


Fig. 5. Maps for several line luminosities ($H\beta$, $[O\text{III}]\lambda 5007$, $H\alpha$, $[N\text{II}]\lambda\lambda 6549, 6583$, and $[S\text{II}]\lambda\lambda 6716, 6731$ from left to right) for our sample. Gray circles denote fibers for which line luminosity could not be estimated due to poor SN. North is up and east is left in all images.

properties that are relevant to the conclusion of this work (see Section 3.3).

Figure 6 shows a spatially resolved BPT diagram (Baldwin et al. 1981) in which each fiber position is classified as Seyfert 2 (Sy2), low-ionization nuclear emission-line region (LINER), composite, star-forming region (SF), and Unknown. We employed diagnostics with line ratios of $[\text{N II}]\lambda 6583/\text{H}\alpha$ and $[\text{O III}]\lambda 5007/\text{H}\beta$ provided by Kauffmann et al. (2003) and Kewley et al. (2006) (see also Toba et al. 2013; Toba et al. 2014), in which narrow component of each emission line is used. If we define a fiber with Sy2 or composite classification as AGN-dominated, NGC 1614, CGCG 468-002W, Mrk 273, and NGC 7674 are AGN-dominated with 50-70% of fibers being classified as Sy2/Composite. For NGC 3690 West and East (that is classified as merger stage C), about 50% and 30% of fibers are classified as AGN, respectively, which suggests that NGC 3690 is basically SF-dominated, but the AGN contribution to the West part is larger than that of the East part for NGC 3690. Indeed, Alonso-Herrero et al. (2000) reported an interaction-induced star formation for this system. Hard X-ray observations also supported the presence of AGN in NGC 3690 West and the absence of AGN (or very faint AGN) in NGC 3690 East (Yamada et al. 2021). A caution here is that obscured AGN often lacks the signature of AGN emission from narrow-line regions (NLRs) in optical spectra because NLR is not well developed, and hence those are even outside of the AGN region in the BPT diagram (Hickox & Alexander 2018, and references therein), which makes the diagnostics with line ratios difficult.

3.3 Outflow properties as a function of distance from the galaxy center

We examine the spatial correlation of outflow properties in a galaxy and how the outflow strength could be associated with the merger stage. The velocity offset and/or velocity dispersion of $[\text{O III}]\lambda 5007$ have been preferentially used for evaluating the strength of ionized gas outflow from the rest-frame optical spectra (e.g., Zakamska et al. 2016; Rakshit & Woo 2018; Chen et al. 2019; Jun et al. 2020). But it is known that the velocity offset or velocity dispersion alone is not always a good tracer of the strength of AGN outflows because they are often affected by dust extinction (Bae & Woo 2014; Woo et al. 2016). To make a fair comparison of outflow power for objects in any merger stage that may have different amounts of dust (e.g., Ricci et al. 2017; Blecha et al. 2018; Ricci et al. 2021; Yamada et al. 2021), we employ the following quantity;

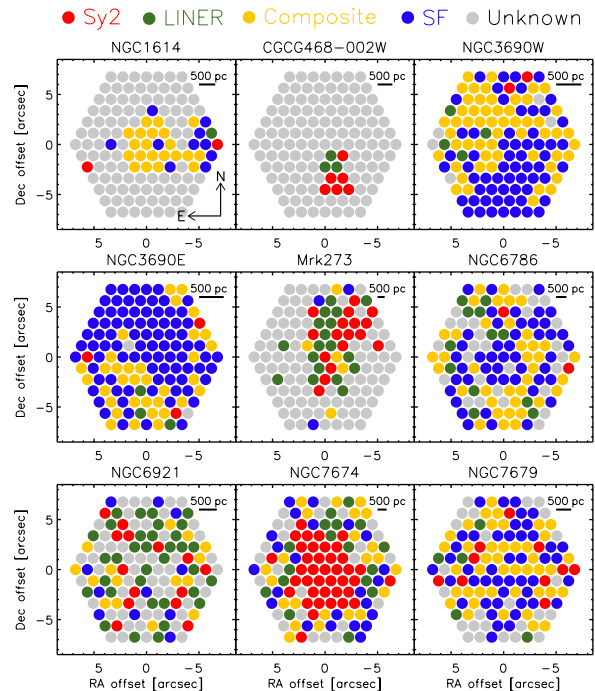


Fig. 6. Spatially resolved BPT diagram for our sample. Red, green, yellow, and blue circles correspond to Sy2, LINER, composite, and SF, respectively. Gray circles denote “Unknown” fibers for which line ratio diagnostics could not be executed because either or both lines for line ratio were undetected. North is up and east is left in all images.

$$\sigma_0 = \sqrt{v_{[\text{O III}] }^2 + \sigma_{[\text{O III}] }^2}, \quad (1)$$

where $v_{[\text{O III}]}$ and $\sigma_{[\text{O III}]}$ are velocity shifts of the broad blue-wing component and its velocity dispersion, respectively. This quantity minimizes the influence of dust extinction; Bae & Woo (2016) demonstrated that σ_0 does not change significantly regardless of the amount of dust extinction given a bicone inclination by assuming a biconical outflow model (see Bae & Woo 2016 for details). This methodology is applicable even to heavily dust-obscured galaxies (Toba et al. 2017b).

We then investigate how σ_0 could depend on the distance from the galaxy center (i.e., fiber center). In order to obtain reliable σ_0 with a relatively small uncertainty, we estimate σ_0 in the following three annular areas with an inner-outer radius of (i) 0–1 kpc, (ii) 1–2 kpc, and (iii) 2–5 kpc. Figure 7 shows resultant σ_0 as a function of galaxy center for various merger stages. The only object classified as merger stage “B”, CGCG 468–002W, is shown only in the innermost area because σ_0 could not be measured in the outer regions due to poor SN¹². We find a negative correlation between distance from the center and σ_0 regardless of the merger stage, with a coefficient of $r \sim -0.4$

¹²Even in the innermost area, the uncertainty of σ_0 is about 0.3 dex (see Figure 7).

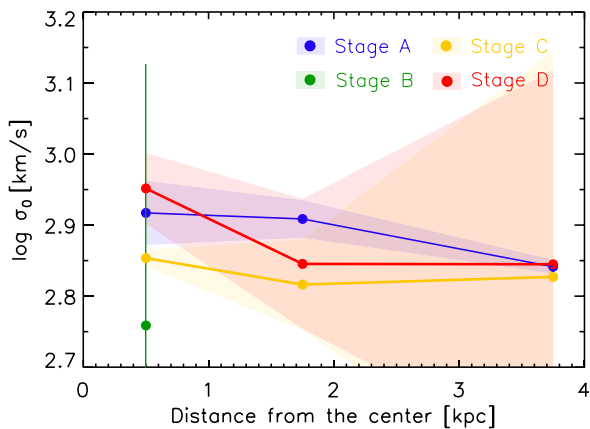


Fig. 7. The outflow strength (σ_0) as a function of the galaxy (fiber) center. Blue, green, yellow, and red data points represent the merger stage of A, B, C, and D, respectively.

in which uncertainties of σ_0 are taken into account (see e.g., Kelly 2007; Toba et al. 2019). This result supports an AGN-driven outflow; an ionized gas outflow is launched from the galactic nucleus. Focusing on the galactic center, σ_0 in merger stage D is the strongest that is comparable to dust-obscured AGN (Toba et al. 2017b) (see also Section 3.4).

It should be noted that a starburst-driven outflow is also reported in some galaxies and is reproduced by numerical simulations (e.g., Jogee et al. 1998; Leon et al. 2007; Schneider et al. 2020). Hence σ_0 may not be tracing purely AGN-driven outflow. To test this possibility, we utilize SDSS spectra of nearby starburst galaxies and execute the spectral analysis. We first select 430 objects from the SDSS DR17 with satisfying the following criteria; (i) $0.01 < z < 0.04$, (ii) $r\text{-mag} < 15$, and (iii) `SUBCLASS = "STARBURST"`¹³. The redshift and magnitude ranges are similar to those in our GOALS sample. The fiber diameter of the SDSS/BOSS Spectrograph is $2''\text{--}3''$, which corresponds to central 2–3 fibers in KOOLS-IFU. We then perform the spectral fitting with `QSFIT` in the same manner as what is described in Section 2.3 and estimate σ_0 . As a result, a weighted mean of σ_0 for the starburst galaxy sample is $\log \sigma_0 \sim 2.7$. This value is smaller than those in the inner part of our GOALS sample, which means that it could be difficult for starburst galaxies to produce such a strong outflow with $\log \sigma_0 > 2.8$ as we observed for our sample (Figure 7). This suggests that high σ_0 basically originates from an AGN-driven outflow.

In order to see how the galaxy merger could affect the gas density from the spatially-resolved view, we also estimate electron density (n_e) of ionized gas from the line flux

ratio of $[\text{S II}]\lambda\lambda 6716, 6731$ that is known as a good tracer of n_e and widely used for AGN¹⁴ (e.g., Osterbrock & Ferland 2006; Kawasaki et al. 2017; Kawaguchi et al. 2018; Joh et al. 2021), which tells us how n_e could be different among the inner and outer regions of our GOALS sample. Here, a conversion formula is employed to estimate n_e from the $[\text{S II}]$ ratio (see e.g., Kakkad et al. 2022, and reference therein). Albeit with a large uncertainty ($\sim 30\%$), we find a spatial gradient of n_e , i.e., high-density gas with $n_e \sim 10^3 \text{ cm}^{-3}$ is located in the central 0.5 kpc while low-density gas with $n_e < 100 \text{ cm}^{-3}$ is distributed in the outer region.

3.4 Outflow properties as a function of merger stage

Finally, we investigate how σ_0 could be associated with the merger stages as shown in Figure 8. We find that ionized gas outflow is more powerful as a sequence of merger stages; the outflow strength in the late-stage (stage D) mergers is about 1.5 times stronger than that in the early-stage (stage B) mergers. We also check the correlation between σ_0 and D_{12} in which D_{12} is the separation between the two nuclei in units of kpc (see Yamada et al. 2021). We confirm a negative correlation between two quantities for samples with merger stages from B to D. We further find that n_e estimated from the $[\text{S II}]$ doublet (see Section 3.3) seems larger in the late-stage merger. Recently, Yamada et al. (2021) reported that the outflow velocity of molecular gas of X-ray AGN in merger stage D correlates with Eddington ratio¹⁵. Molecular outflows are also correlated with ionized gas outflow regarding the mass outflow rate (Fiore et al. 2017). These results suggest that the galaxy merger could induce a dense ionized gas outflow driven by AGN, particularly in the late-stage merger. At the same time, an important caveat to be kept in mind is that those results are based only on nine objects. We cannot rule out the possibility that the observed trends are affected by a selection effect (see below). Further observations for the GOALS sample with a wider range of redshift, brightness, and dynamical state are needed to corroborate our conclusion.

We also note that σ_0 for merger stage A is comparably large to stage D. One possible reason for this is that merger stage A is a too early phase (i.e., two galaxies are too far from each other) to affect the strength of the ionized gas outflow, and thus σ_0 could depend on the nature of the individual object rather than the contribution of the merger process. Indeed, NGC 6921, NGC 7674, and NGC 7679

¹⁴Recently, some caveats of using $[\text{S II}]$ doublet for n_e have been reported (Davies et al. 2020, and references therein).

¹⁵Yamada et al. (2021) also reported a positive correlation between outflow velocity of molecular gas and X-ray bolometric correction that may be correlated with Eddington ratio (see e.g., Toba et al. 2019).

¹³It labels a galaxy with being classified star-forming galaxies (SFGs) in the BPT diagram but has an equivalent width of $\text{H}\alpha$ greater than 50 Å.

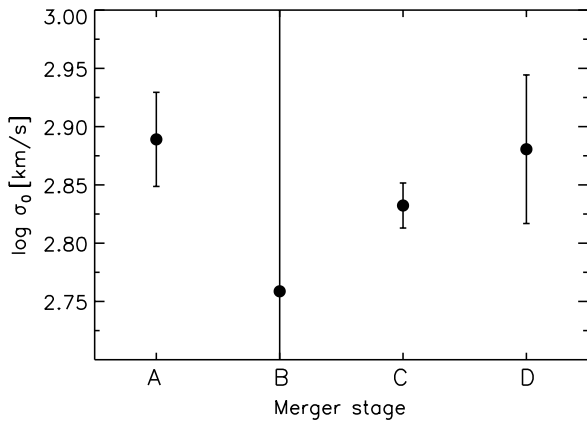


Fig. 8. The outflow strength (σ_0) as a function of the merger stage. Since especially objects classified as stage A might be affected by the selection effect or even classified as stage D, our conclusions are based primarily on results from stage B to D (see the text for details).

(that are classified as merger stage A) are all reported as strong AGNs with X-ray detections¹⁶ (see Yamada et al. 2021, for details). In particular, NGC 7674 is expected to harbor dual SMBHs (Kharb et al. 2017, but see also Breiding et al. 2022 for counterargument), which could have a quite strong AGN outflow¹⁷. A full investigation of this object will be reported (S. Yamada et al. in preparation). Another possibility is that those objects are indeed at the very last stage of former merging events so that no tidal features are visible (which means they are stage D). On the other hand, if the trend in Figure 8 is robust without being affected by the selection effect, this result could suggest that galaxy merger is not the only path to ignite AGN as introduced in Section 1.

Arribas et al. (2014) reported that SF-driven outflow strength traced by H α line in SFGs is correlated with dynamical phases (that corresponds to the merger stage, see Rodríguez-Zaurín et al. 2011, for more detail) along the merging process. Rich et al. (2015) also reported from an IFU observation that the low-velocity shocks become increasingly prominent as a merger progresses (see also Rich et al. 2011). In addition, the outflow strength (σ_0) seems to be correlated with the Eddington ratio (e.g., Bae & Woo 2014; Toba et al. 2017b). Taking account of those findings into account, our observations support that galaxy mergers enhance both SF and AGN activity and play an important role in the co-evolution of galaxies and SMBHs.

¹⁶NGC 7674 and MGC 7679 are also reported [Ne v] λ 14.32 μ m detections (Inami et al. 2013).

¹⁷The Eddington ratio of NGC 7674 is also larger than other AGN in our sample (Yamada et al. 2021).

4 Summary

In order to reveal how the galaxy merger could affect the strength of the ionized gas outflow from a spatially-resolved point of view, we analyze 9 local U/LIRGs at $z < 0.04$ through the IFU observations with KOOLS-IFU on Seimei Telescope. The observed targets are selected from a 60 μ m flux-limited sample in the GOALS project, covering a wide range of merger states from an early-stage (A) to late-stage (D). We successfully detect various emission lines of H β , [O III] $\lambda\lambda$ 4959,5007, H α , [N II] $\lambda\lambda$ 6549,6583, and [S II] $\lambda\lambda$ 6716,6731 over 70% of fibers. This work mainly focuses on the strength of the ionized gas outflow (σ_0) by using a combination of velocity shift and dispersion of [O III] λ 5007 line. With all the caveats discussed in Sections 3.3 and 3.4 in mind, we find σ_0 shows a negative correlation with the distance from the galaxy center and a positive correlation with a sequence of merger stages. This indicates that galaxy mergers may induce AGN-driven outflow and maximize the late-stage merger, which is in good agreement with previous works reporting that the Eddington ratio of AGN increases along with the merger stage.

Since our follow-up observation campaign with KOOLS-IFU is ongoing, and about 130 GOALS samples are observable from the Seimei telescope, this work provides a benchmark for revealing the spatially-resolved outflow properties from a static point of view in the future.

Acknowledgments

We gratefully thank the anonymous referee for a careful reading of the manuscript and very helpful comments. We acknowledge Dr. Kyuseok Oh for providing a finding chart for our observations in 2019. This work is supported by JSPS KAKENHI Grant numbers 18J01050, 19K14759, and 22H01266 (YT), 19J22216 (SY), 20H01946 (YU), and 20K04027 (NO). SY is grateful for support from RIKEN Special Postdoctoral Researcher Program.

References

- Abdurro'uf, et al., 2022, ApJS, 259, 35
- Alonso-Herrero, A., Rieke, G. H., Rieke, M. J., & Scoville, N. Z. 2000, ApJ, 532, 845
- Alonso-Herrero, A., García-Marín, M., Monreal-Ibero, A., Colina, L., Arribas, S., Alfonso-Garzón, J., & Labiano, A. 2009, A&A, 506, 1541
- Armus, L., et al. 2009, PASP, 121, 559
- Armus L., Charmandaris V., & Soifer B. T., 2020, Nat. Astron., 4, 467
- Arribas, S., Colina, L., Monreal-Ibero, A., Alfonso, J., García-Marín, M., & Alonso-Herrero, A. 2008, A&A, 479, 687
- Arribas, S., Colina, L., Bellocchi, E., Maiolino, R., & Villar-Martín, M. 2014, A&A, 568, A14,
- Bae, H.-J., & Woo, J.-H. 2014, ApJ, 795, 30

- Bae, H.-J., & Woo, J.-H. 2016, *ApJ*, 828, 97
- Bae, H.-J., Woo, J.-H., Karouzos, M., Gallo, E., Flohic, H., Shen, Y., & Yoon, S.-J. 2017, *ApJ*, 837, 91
- Baldwin J. A., Phillips M. M., Terlevich R., 1981, *PASP*, 93, 5
- Barcos-Muñoz, L., et al. 2017, *ApJ*, 843, 117
- Barden, S. C., Armandroff, T., Muller, G., Rudeen, A. C., Lewis, J., & Groves, L. 1994, *Proc. SPIE*, 2198, 87
- Barden, S. C., & Armandroff, T. 1995, *Proc. SPIE*, 2476, 56
- Bellocchi, E., Arribas, S., Colina, L., & Miralles-Caballero, D. 2013, *A&A*, 557, A59
- Bischetti, M., et al. 2017, *A&A*, 598, A122
- Blecha, L., Snyder, G. F., Satyapal, S., & Ellison, S. L. 2018, *MNRAS*, 478, 3056
- Breiding, P., Burke-Spolaor, S., An, T., Bansal, K., Mohan, P., Taylor, B. G., & Zhang, Y. 2022, *ApJ*, 933, 143
- Bryant, J. J., et al. 2015, *MNRAS*, 447, 2857
- Bundy, K., et al. 2015, *ApJ*, 798, 7
- Calderone, G., Nicastro, L., Ghisellini, G., Dotti, M., Sbarrato, T., Shankar, F., & Colpi, M., 2017, *MNRAS*, 472, 4051
- Casey, C. M. 2012, *MNRAS*, 425, 3094
- Cazzoli, S., Arribas, S., Maiolino, R., & Colina, L., 2016, *A&A*, 590, A125
- Chambers, K. C., et al. 2016, arXiv:1612.05560
- Chary, R., & Elbaz, D. 2001, *ApJ*, 556, 562
- Chen, X., et al. 2019, *PASJ*, 71, 29
- Chu, Jason K., et al. 2017, *ApJS*, 229, 25,
- Condon, J. J., Cotton, W. D., Jarrett, T., Marchetti, L., Matthews, A. M., Mauch, T., & Moloko, M. E. 2021, *ApJS*, 257, 35
- Conselice, C. J. 2014, *ARA&A*, 52, 291
- Croom, S. M., et al. 2021, *MNRAS*, 505, 991
- Davies R. et al., 2020, *MNRAS*, 498, 4150
- de Zeeuw, P. T., et al. 2002, *MNRAS*, 329, 513
- Díaz-Santos, T., et al. 2017, *ApJ*, 846, 32
- Dietrich M., Appenzeller I., Vestergaard M., & Wagner S. J., 2002, *ApJ*, 564, 581
- Draper, A. R., & Ballantyne, D. R. 2012, *ApJ*, 751, 72
- Finnerty, L., et al. 2020, *ApJ*, 905, 16
- Fiore, F., et al. 2017, *A&A*, 601, A143
- Fluetsch, A., et al. 2021, *MNRAS*, 505, 5753
- García-Marín, M., Colina, L., Arribas, S., Alonso-Herrero, A., & Mediavilla, E. 2006, *ApJ*, 650, 850
- García-Marín, M., Colina, L., Arribas, S., & Monreal-Ibero, A. 2009, *A&A*, 505, 1319
- Grandi S. A., 1982, *ApJ*, 255, 25
- Haan, S., et al. 2011, *ApJS*, 197, 27
- Harrison, C. M., Costa, T., Tadhunter, C. N., Flütsch, A., Kakkad, D., Perna, M. & Vietri, G. 2018, *Nature Astron.*, 2, 198
- Herrero-Illana, R., et al. 2019, *A&A*, 628, A71
- Hickox, R. C., & Alexander, D. M. 2018, *ARA&A*, 56, 625
- Howell, J. H., et al. 2010, *ApJ*, 715, 572
- Imanishi, M., Dudley, C. C., Maiolino, R., Maloney, P. R., Nakagawa, T., & Risaliti, G. 2007, *ApJS*, 171, 72
- Imanishi, M. 2009, *ApJ*, 694, 751
- Inami, H., et al. 2013, *ApJ*, 777, 156
- Inami, H., et al. 2018, *A&A*, 617, A130
- Iwasawa, K., et al. 2011, *A&A*, 529, A106
- Jin, J.-J., Zhu, Y.-N., Wu, H., Lei, F.-J., Cao, C., Meng, X.-M., Zhou, Z.-M., & Lam, M. I. 2019, *ApJS*, 244, 33
- Jogee, S., Kenney, J. D. P., & Smith, B. J. 1998, *ApJ*, 494, 185
- Joh, K., Nagao, T., Wada, K., Terao, K., & Yamashita, T. 2021, *PASJ*, 73, 1152
- Jun, H. D., et al. 2020, *ApJ*, 888, 110
- Kakkad, D., et al. 2022, *MNRAS*, 511, 2105
- Kauffmann, G., et al. 2003, *MNRAS*, 346, 1055
- Kawaguchi, T., et al. 2018, *PASJ*, 70, 93
- Kawasaki, K., Nagao, T., Toba, Y., Terao, K., & Matsuoka, K. 2017, *ApJ*, 842, 44
- Kelly B. C., 2007, *ApJ*, 665, 1489
- Kewley, L. J., Groves, B., Kauffmann, G., & Heckman, T. 2006, *MNRAS*, 372, 961
- Kharb, P., Lal, D. V., & Merritt, D. 2017, *Nat. Astron.*, 1, 727
- Kim, D.-C., et al. 2013, *ApJ*, 768, 102
- Kurita, M., et al. 2020, *PASJ*, 72, 48
- Larson, K. L., et al. 2020, *ApJ*, 888, 92
- Leon, S., et al. 2007, *A&A*, 473, 747
- Linden, S. T., et al. 2017, *ApJ*, 843, 91
- Linden, S. T., et al. 2019, *ApJ*, 881, 70
- Markwardt, C. B. 2009, *ASP Conf. Ser.*, 411, 251
- Matsubayashi, K., et al. 2019, *PASJ*, 71, 102
- Narayanan, D., et al. 2010, *MNRAS*, 407, 1701
- Osterbrock, D. E., & Ferland, G. J. 2006, *Astrophysics of Gaseous Nebulae and Active Galactic Nuclei*, 2nd ed. (Sausalito, CA: University Science Books)
- Pan, H.-A., et al. 2019, *ApJ*, 881, 119
- Perna, M., et al. 2021, *A&A*, 646, A101
- Perna, M., et al. 2022, *A&A*, 662, A94
- Petty, S. M., et al. 2014, *AJ*, 148, 111
- Piqueras López, J., Colina, L., Arribas, S., Alonso-Herrero, A., & Bedregal, A. G. 2012, *A&A*, 546, A64
- Polletta, M., et al. 2007, *ApJ*, 663, 81
- Privon, G. C., et al. 2015, *ApJ*, 814, 39
- Rakshit, S., & Woo, J.-H. 2018, *ApJ*, 865, 5
- Ricci, C., et al. 2017, *MNRAS*, 468, 1273
- Ricci, C., et al. 2021, *MNRAS*, 506, 5935
- Rich, J. A., Kewley, L. J., & Dopita, M. A. 2011, *ApJ*, 734, 87
- Rich, J. A., Torrey, P., Kewley, L. J., Dopita, M. A., & Rupke, D. S. N. 2012, *ApJ*, 753, 5
- Rich, J. A., Kewley, L. J., & Dopita, M. A. 2015, *ApJS*, 221, 28
- Rodríguez-Zaurín, J., Arribas, S., Monreal-Ibero, A., Colina, L., Alonso-Herrero, A., & Alfonso-Garzón, J. 2011, *A&A*, 527, A60
- Sánchez, S. F., et al. 2012, *A&A*, 538, A8
- Sánchez, S. F., et al. 2016, *A&A*, 594, A36
- Sanders, D. B., & Mirabel, I. F. 1996, *ARA&A*, 34, 749
- Sanders D. B., Soifer B. T., Elias J. H., Madore B. F., Matthews K., Neugebauer G., & Scoville N. Z., 1988, *ApJ*, 325, 74
- Sanders, D. B., Mazzarella, J. M., Kim, D., Surace, J. A., & Soifer, B. T. 2003, *AJ*, 126, 1607
- Schawinski, K., Treister, E., Urry, C. M., Cardamone, C. N., Simmons, B., & Yi, S. K. 2011, *ApJ*, 727, L31
- Schlafly, E. F., & Finkbeiner, D. P. 2011, *ApJ*, 737, 103
- Schneider, E. E., Ostriker, E. C., Robertson, B. E., &

- Thompson, T. A. 2020, *ApJ*, 895, 43
- Science Software Branch at STScI 2012, *Astrophysics Source Code Library*, ascl:1207.011
- Sharma, R. S., et al. 2021, (arXiv:2101.01729)
- Shin J., Woo J.-H., Chung A., Baek J., Cho K., Kang D., & Bae H.-J., 2019, *ApJ*, 881, 147
- Stierwalt, S., et al. 2013, *ApJS*, 206, 1
- Stierwalt, S., et al. 2014, *ApJ*, 790, 124
- Toba, Y., et al. 2013, *PASJ*, 65, 113
- Toba, Y., et al. 2014, *ApJ*, 788, 45
- Toba, Y., et al. 2015, *PASJ*, 67, 86
- Toba, Y., & Nagao, T. 2016, *ApJ*, 820, 46
- Toba, Y., et al. 2017a, *ApJ*, 840, 21
- Toba, Y., Bae, H.-J., Nagao, T., Woo, J.-H., Wang, W.-H., Wagner, A. Y., Sun, A.-L., & Chang, Y.-Y. 2017b, *ApJ*, 850, 140
- Toba, Y., Komugi, S., Nagao, T., Yamashita, T., Wang, W.-H., Imanishi, M., & Sun, A.-L. 2017c, *ApJ*, 851, 98
- Toba, Y., Ueda, Y., Matsuoka, K., Shidatsu, M., Nagao, T., Terashima, Y., Wang, W.-H., & Chang, Y.-Y. 2019, *MNRAS*, 484, 196
- Toba, Y., et al. 2021a, *ApJ*, 912, 91
- Toba, Y., et al. 2021b, *A&A*, 649, L11
- Tody, D. 1986, *Proc. SPIE*, 627, 733
- Tody, D. 1993, in *ASP Conf. Ser. 52, Astronomical Data Analysis Software and Systems II*, ed. R. J. Hanisch, R. J. V. Brissenden, & J. Barnes (San Francisco, CA: ASP), 173
- Torres-Albà, N., et al. 2018, *A&A*, 620, A140
- U, V., et al. 2012, *ApJS*, 203, 9
- U, V., et al. 2019, *ApJ*, 871, 166
- Veilleux, S., Kim, D.-C., & Sanders, D. B. 2002, *ApJS*, 143, 315
- Véron-Cetty, M.-P., Joly M., & Véron P., 2004, *A&A*, 417, 515
- Vestergaard, M., & Wilkes B. J., 2001, *ApJS*, 134, 1
- Woo, J.-H., Bae, H.-J., Son, D., & Karouzos, M. 2016, *ApJ*, 817, 108
- Yamada S., Ueda Y., Tanimoto A., Kawamuro T., Imanishi M., & Toba Y., 2019, *ApJ*, 876, 96
- Yamada S., Ueda Y., Tanimoto A., Oda S., Imanishi M., Toba Y., & Ricci C., 2020, *ApJ*, 897, 107
- Yamada S., Ueda Y., Tanimoto A., Imanishi M., Toba Y., Ricci C., & Privon G. C., 2021, *ApJS*, 257, 61
- Yamashita, T., et al. 2017, *ApJ*, 844, 96
- York, D. G., et al. 2000, *AJ*, 120, 1579
- Yoshida, M. 2005, *J. Korean Astron. Soc.*, 38, 117
- Zakamska, N. L., et al. 2016, *MNRAS*, 459, 3144